Plasma Power Source Based on a Catalytic Reaction of Atomic Hydrogen

R. L. Mills, P. Ray, B. Dhandapani, J. Dong, S. Hicks, M. Nansteel, X. Chen, J. He, R. Mayo
BlackLight Power, Inc.
493 Old Trenton Road
Cranbury, NJ 08512

ABSTRACT

Extreme ultraviolet (EUV) spectroscopy was recorded on microwave discharges of helium with 2% hydrogen. Novel emission lines were observed with energies of $q \cdot 13.6\,eV$ where $q = 1,2,3,4,6,7,8,9,11$ or these lines inelastically scattered by helium wherein $21.2\,eV$ was absorbed in the excitation of $He\,(1s^2)$ to $He\,(1s^1 2p^1)$. The average hydrogen atom temperature was measured to be $180 - 210\,eV$ versus $\approx 3\,eV$ for pure hydrogen. The electron temperature T_e for helium-hydrogen was 28,000 K compared to 6800 K for pure helium. Using heat loss and Calvet calorimetry, excess power was observed from the helium-hydrogen plasma compared to control xenon or krypton plasmas. For example, for an input of 22 W, the total plasma power of the helium-hydrogen plasma measured by Calvet calorimetry was 60 W corresponding to 38 W of excess power in 0.32 cm^3. The excess power density and energy balance were very high, 120 W/cm^3 and $-1.3\,X\,10^5\,kJ/mole\,H_2$, respectively.

1. Introduction

A new chemically generated or assisted plasma source has been developed that is based on a resonant energy transfer mechanism (rt-plasma). One such source operates by incandescently heating a hydrogen dissociator and a catalyst to provide atomic hydrogen and gaseous catalyst, respectively, such that the catalyst reacts with the atomic hydrogen to produce a plasma. It was extraordinary, that intense EUV emission was observed by Mills et al. [1] at low temperatures (e.g. $\approx 10^3\ K$) and an extraordinary low field strength of about 1-2 V/cm from atomic hydrogen and certain atomized elements or certain gaseous ions which singly or multiply ionize at integer multiples of the potential energy of atomic hydrogen, $27.2\ eV$. A number of independent experimental observations confirm that the rt-plasma is due to a novel reaction of atomic hydrogen which produces as chemical intermediates, hydrogen in fractional quantum states that are at lower energies than the traditional "ground" ($n=1$) state. Power is released, and the final reaction products are novel hydride compounds. The supporting data include EUV spectroscopy [1-8], characteristic emission from catalysts and the hydride ion products [4], lower-energy hydrogen emission [2-4, 7-8], chemically formed plasmas [1, 4-6], Balmer α line broadening [7-11], anomalous plasma afterglow duration [6], power generation [5, 7-9, 11-12], and analysis of novel chemical compounds [13].

The reaction has applications as a new light source, a new field of hydrogen chemistry, and a new source of energy. Since the power is in the form of a plasma, direct plasma to electric power conversion is possible. Plasmadynamic conversion of microwave plasma power to electricity has been achieved at about 1.61 W/ cm^3 with about 18.8 % efficiency [14].

The theory given previously [15-17] is based on applying Maxwell's equations to the Schrödinger equation. The familiar Rydberg equation (Eq. (1)) arises for the hydrogen excited states for $n>1$ of Eq. (2).

$$E_n = -\frac{e^2}{n^2 8\pi\varepsilon_o a_H} = -\frac{13.598\ eV}{n^2} \tag{1}$$

$$n = 1,2,3,... \tag{2}$$

An additional result is that atomic hydrogen may undergo a catalytic

reaction with certain atoms and ions which singly or multiply ionize at integer multiples of the potential energy of atomic hydrogen, $m \cdot 27.2\ eV$ wherein m is an integer. The reaction involves a nonradiative energy transfer to form a hydrogen atom that is lower in energy than unreacted atomic hydrogen that corresponds to a fractional principal quantum number. That is

$$n = \frac{1}{2}, \frac{1}{3}, \frac{1}{4}, \ldots, \frac{1}{p}; \quad p \text{ is an integer} \tag{3}$$

replaces the well known parameter $n = \text{integer}$ in the Rydberg equation for hydrogen excited states. The $n = 1$ state of hydrogen and the $n = \frac{1}{\text{integer}}$ states of hydrogen are nonradiative, but a transition between two nonradiative states, say $n = 1$ to $n = 1/2$, is possible via a nonradiative energy transfer. Thus, a catalyst provides a net positive enthalpy of reaction of $m \cdot 27.2\ eV$ (i.e. it resonantly accepts the nonradiative energy transfer from hydrogen atoms and releases the energy to the surroundings to affect electronic transitions to fractional quantum energy levels). As a consequence of the nonradiative energy transfer, the hydrogen atom becomes unstable and emits further energy until it achieves a lower-energy nonradiative state having a principal energy level given by Eqs. (1) and (3). Processes such as hydrogen molecular bond formation that occur without photons and that require collisions are common [18]. Also, some commercial phosphors are based on resonant nonradiative energy transfer involving multipole coupling [19].

We propose that atomic hydrogen may undergo a catalytic reaction with He^+ which ionizes at two times the potential energy of atomic hydrogen, $2 \cdot 27.2\ eV$. Thus, microwave discharges of helium-hydrogen mixtures were studied by EUV spectroscopy to search for line emission from transitions to fractional Rydberg states of atomic hydrogen. Since the electronic transitions are very energetic, Balmer α line broadening, electron temperature, and power balances were measured to determine whether this reaction has sufficient kinetics to merit its consideration as a practical power source.

2. Experimental

EUV spectroscopy was recorded on hydrogen, xenon, helium, xenon-hydrogen (98/2%), and helium-hydrogen (98/2%) microwave discharge plasmas (Opthos, Model MPG-4M, Frequency: 2450 MHz) according to the methods given previously [2]. A xenon-hydrogen (98/2%) or helium-hydrogen (98/2%) gas mixture was flowed at 1 Torr or 20 Torr through a half inch diameter quartz tube fitted with an Evenson cavity, and each plasma of hydrogen, xenon, and helium alone was run at 20 Torr. The input power to the plasma was set at 85 W with forced air cooling of the cell. The spectrometer was a normal incidence 0.2 m monochromator equipped with a 1200 lines/mm holographic grating with a platinum coating that covered the region $2-560\,nm$. The EUV spectrum was recorded with a CEM. The wavelength resolution was about $0.02\,nm$ (FWHM) with slit widths of $50\,\mu m$. The increment was $0.2\,nm$ and the dwell time was $500\,ms$. Peak assignments were based on a calibration against the known He I and He II lines.

To achieve higher sensitivity at the shorter EUV wavelengths, the light emission from plasmas of helium alone was recorded with a 4° grazing incidence EUV spectrometer equipped with a grating having 600 G/mm with a radius of curvature of $\approx 1\,m$ that covered the region $5-65\,nm$. The angle of incidence was 87°. The resolution was about $0.04\,nm$ (FWHM) with slit widths of $300\,\mu m$. A CEM was used to detect the EUV light. The increment was $0.1\,nm$ and the dwell time was $1\,s$.

The width of the 656.3 nm Balmer α line emitted from hydrogen alone, xenon-hydrogen mixture (90/10)%, and helium-hydrogen mixture (90/10)% microwave discharge plasmas was measured with a high resolution visible spectrometer capable of a resolution of $\pm 0.006\,nm$ [10]. In this case, the total pressure was 1 Torr, and the input power to the plasma was set at 40 W.

T_e was measured on 0.1 Torr microwave plasmas of helium alone and helium-hydrogen mixtures (90/10%) from the ratio of the intensity of the *He* 501.6 nm (upper quantum level n=3) line to that of the *He* 492.2 nm (n=4) line as described by Griem [20]. T_e was measured on hydrogen alone plasmas from their Balmer line intensities. The visible spectrum $400-560\,nm$ was recorded with the normal incidence EUV

spectrometer using a PMT and a sodium salicylate scintillator.

The excess power generated by the microwave initiated rt-plasma was measured by heat loss calorimetry. The technique relies on measuring the conductive thermal power flow through the cell wall to the constant temperature environment by recording the temperature over the cell wall external to the reaction. In this case, the heat flow is independent of processes that occur inside of the cell. The temperature profile of the catalyst case is compared to that of a control case, and the excess power is calculated based on the greater power loss to the ambient environment based on the higher temperature profile with the catalyst-hydrogen over the noncatalyst plasma.

The general system design of the heat loss calorimeter is shown in Figure 1. The external wall temperature of the 1.27 cm I.D. quartz tube was measured with 6 beaded thermocouples (Type K) attached to the cell wall with high-temperature, microwave-transparent cement. The thermocouples were linearly spaced, 2 cm apart from the position 2 cm negative of the center over an 8 cm span as shown in Figure 2. An Evenson cavity was placed over the center thermocouple such that the temperature profile was recorded from one half of the cell as well as the -2 cm position. The external-wall temperature profile was shown to be azimuthally symmetrical by rotating the microwave cavity, and the temperature profile was shown to be symmetrical about the center in repeated separate experiments. Thus, due to the symmetry, the thermocouple response was representative of the temperature profile of the entire cell.

The temperature response was tested with the cell under vacuum (i.e. no gas) to measure the absorption of microwaves by the quartz cell and the thermocouples and to measure any possible microwave electrical interference with the thermocouples. The temperature rise resulting from 40 W microwave input power was negligible (<1°C even at the center).

Catalyst and noncatalyst microwave plasmas of premixed helium with 5% hydrogen and krypton alone, respectively, were maintained with a constant 30 W input to the Evenson cavity in an approximately 10 cm^3 plasma volume of the quartz microwave cell. The input power was confirmed by a microwave power meter (Thruline Wattmeter, Bird

Electronic Corp., Model 43, 2400-2500 MHz 50W slug). The input power was essentially 100% dissipated inside the cell since the microwave leakage was measured to be less than 100 mW with a microwave survey meter (Holaday Industries, Inc., 2450 MHz, HI-1501). The pressure of the ultrahigh pure gas or gas mixture inside the cell was maintained at about 500 mTorr with a gas flow rate of 3 sccm controlled by a mass flow controller.

The general form of the energy balance equation for the cell in steady state is:

$$0 = Q_{in} + Q_{ex} - Q_{loss} \tag{4}$$

where Q_{in} is the input power to the microwave discharge, Q_{ex} is the excess power generated from the hydrogen catalysis reaction, and Q_{loss} is the thermal power loss from the cell. ΔT, the local temperature rise of the tube surface above the ambient temperature was given by

$$\Delta T = T - T_{\infty} \tag{5}$$

where the ambient temperature was $T_{\infty} = 23.4°C$. At the same input power, the ΔT cell response profile was determined for the test and control gases after each cell had reached a thermal steady state. The time to reach a steady state temperature was about 5 minutes. At this point, the power lost from the cell Q_{loss} was equal to the total power Q_T which in turn equaled the power supplied to the cell Q_{in} plus any excess power Q_{ex}.

$$Q_T = Q_{in} + Q_{ex} = Q_{loss} \tag{6}$$

A lower bound for the total plasma tube heat loss Q_T of the catalyst-hydrogen plasma is developed in Sec. IIIC. The model is based on determining the ratio of the heat loss of the catalyst-hydrogen plasma to that of the control. The higher temperature produced by the catalyst gases compared with the control gases was representative of the excess power since the cell temperature rise was found to be insensitive to heat transfer mechanisms occurring inside of the cell—the transfer to the cell walls being very fast and heat loss from the wall to the outside ambient environment dominating the cell temperature. Since $Q_T = Q_{in}$ for the control, Q_T for the catalyst-hydrogen plasma was determined by multiplying the ratio by Q_{in}. The excess power P_{ex} was determined from Eq. (6).

The power balance of the helium-hydrogen plasma compared to a

control plasma was also measured by Calvet calorimetry. The instrument used to measure the heat of reaction was a cylindrical heat flux calorimeter (International Thermal Instrument Co., Model CA-100-1). The cylindrical calorimeter walls contained a thermopile structure composed of two sets of thermoelectric junctions. One set of junctions was in thermal contact with the internal calorimeter wall, at temperature T_i, and the second set of thermal junctions was in thermal contact with the external calorimeter wall at T_o. The temperature of the environment was held constant by a forced convection oven. When heat was generated in the calorimeter cell, the calorimeter radially transferred a constant fraction of this heat into the surrounding heat sink. As heat flowed a temperature gradient, $(T_i - T_o)$, was established between the two sets of thermopile junctions. This temperature gradient generated a voltage which was compared to the linear voltage versus power calibration curve to give the power of reaction.

A schematic showing series-connected thermo-elements to illustrate the operating principle of a Calvet calorimeter is shown in Figure 3. For N pairs of thermo-elements, the voltage V is given by the integral of the Seebeck coefficient σ over the temperature change for thermo-elements A and B.

$$V = N\left(\int_{T_o}^{T_i} \sigma_A dT + \int_{T_i}^{T_o} \sigma_B dT\right) = N\int_{T_o}^{T_i} (\sigma_A - \sigma_B) dT \tag{7}$$

$$= N\int_{T_o}^{T_i} \sigma_{AB} dT \tag{8}$$

Here T_i is the temperature at the inner element and T_o is the temperature at the outer element. The relative Seebeck coefficient for the thermo-element pair is constant over a small temperature range. Thus,

$$V = N\sigma_{AB}(T_i - T_o) \propto Q = \text{heat flow rate} \tag{9}$$

To increase the rate of reaction which was determined previously to be temperature dependent, the calorimeter was placed inside a commercial forced convection oven (Precision Scientific 625 S) that was operated at 325 K. The oven also served to maintain an isothermal reaction system and improve baseline stability. A more complete description of a similar Calvet instrument and methods are given by Bradford, Phillips, and Klanchar [21]. The general system design of the

Calvet calorimeter is shown in Figure 4.

The cross section of the Calvet calorimeter with a Beenakker microwave cavity in insitu shown along the axis of the cavity is shown in Figure 5. A 5 mm O.D., 3 mm I.D. quartz plasma chamber was inserted in the 5 in. in diameter, copper Beenakker microwave resonant cavity (Opthos, 2450 MHz) as shown in Figure 6. A new quartz tube was used for each experiment since it was determined that chemicals generated by a catalyst-hydrogen mixture could produce heat during control runs. Test gases comprised control, xenon alone, and a premixed helium-hydrogen mixture (95/5%). The pressure of the ultrahigh purity gas (Praxair) inside the cell was maintained at about 500 mTorr with a xenon gas flow rate of 2.0 sccm or a helium-hydrogen flow rate of 8.0 sccm controlled by a mass flow controller and by adjusting the pumping. The plasma was started outside of the Calvet cup with a Helmholtz coil and maintained with the Opthos generator. A high temperature coaxial cable (RG2250) was used to deliver power from the Opthos microwave generator to the microwave cavity operated at the higher temperature. The power was set at the desired level while minimizing the reflected power with the tuning stubs. The input power read from the power meters of the Opthos generator was confirmed with the microwave power meter. The cavity was placed in the Calvet cup, thermocouples were attached to monitor the cavity temperature, and the cavity was completely packed in aluminum shot. The highly thermally conductive shot provided efficient thermal coupling of the cavity to the Calvet calorimeter. The oven was started, and a steady state Calvet signal was reached after 20-24 hours. The calorimeter was calibrated with the xenon plasma run under identical conditions as the helium-hydrogen plasma. The data was recorded with a PC based computer data acquisition system (National Instruments).

Since the ambient temperature was held constant, the general form of the energy balance equation for the cell in steady state is given by Eq. (4). The Calvet voltage response was recorded after the cell had reached a thermal steady state. At this point, the power lost from the cell Q_{loss} was equal to the total power Q_T which in turn equaled the power supplied to the cell Q_{in} plus any excess power Q_{ex} as given by Eq. (6). Since the heat transfer was dominated by conduction, the output voltage

of the cell V was modeled by a linear fit

$$V = aQ_T \tag{10}$$

where a is a constant determined from the Calvet voltage response V to a given power input for the control experiment ($Q_{ex} = 0$). The higher voltage produced by the helium-hydrogen plasma compared with the control xenon was representative of the excess power. In the case of the catalyst run, the total output power Q_T was determined by solving Eq. (10) using the measured V. The excess power Q_{ex} was determined from Eq. (6).

3. Results and discussion

A. EUV Spectroscopy

In the case of the EUV spectrum of hydrogen, xenon, or xenon-hydrogen (98/2%), no peaks were observed below 78 *nm*, and no spurious peaks or artifacts due to the grating or the spectrometer were observed. Only known He I and He II peaks were observed in the EUV spectrum of the control helium microwave discharge cell emission.

The EUV spectra (17.5 - 50 *nm*) of the microwave cell emission of the helium-hydrogen mixture (98/2%) (top curve) and the helium control (bottom curve) are shown in Figure 7. Ordinary hydrogen has no emission in these regions. Novel peaks were observed at 45.6 *nm*, 37.4 *nm*, and 20.5 *nm* which do not correspond to helium. At the 1 Torr condition, additional novel peaks were observed in the short wavelength region (5 - 65 *nm*) at 14.15 *nm*, 13.03 *nm*, 10.13 *nm*, and 8.29 *nm* which do not correspond to helium as shown in Figure 7. Known He I lines which were used for calibration of the novel peak positions were observed at 58.4 *nm*, 53.7 *nm*, and 52.4 *nm*. It is proposed that the 30.4 *nm* peak shown in Figures 7 and 8 was not entirely due to the He II transition. In the case of the helium-hydrogen mixture, the ratio of 30.4 *nm* (40.8 *eV*) peak to the 25.6 *nm* (48.3 *eV*) was 10 compared to 5.4 for helium alone as shown in Figure 7 which implies only a minor He II transition contribution to the 30.4 *nm* peak.

It is proposed that the majority of the 91.2 *nm* peak was also due to a novel transition. At 20 Torr, the ratio of the Lyman β peak to the

91.2 *nm* peak of the helium-hydrogen plasma was 2 compared to 8 for each control hydrogen and xenon-hydrogen plasma which indicates that the majority of the 91.2 *nm* peak was due to a transition other than the binding of an electron by a proton.

The novel peaks fit two empirical relationships. In order of energy, the set comprising the peaks at 91.2 *nm*, 45.6 *nm*, 30.4 *nm*, 13.03 *nm*, 10.13 *nm*, and 8.29 *nm* correspond to energies of $q \cdot 13.6\ eV$ where $q = 1,2,3,7,9,11$. In order of energy, the set comprising the peaks at 37.4 *nm*, 20.5 *nm*, and 14.15 *nm* correspond to energies of $q \cdot 13.6 - 21.21\ eV$ where $q = 4,6,8$. These lines can be explained as electronic transitions to fractional Rydberg states of atomic hydrogen given by Eqs. (1) and (3) wherein the catalytic system involves helium ions because the second ionization energy of helium is $54.417\ eV$, which is equivalent to $2 \cdot 27.2\ eV$. In this case, $54.417\ eV$ is transferred nonradiatively from atomic hydrogen to He^+ which is resonantly ionized. The electron decays to the $n = 1/3$ state with the further release of $54.417\ eV$ which may be emitted as a photon. The catalysis reaction is

$$54.417\ eV + He^+ + H[a_H] \rightarrow He^{2+} + e^- + H\left[\frac{a_H}{3}\right] + 108.8\ eV \tag{11}$$

$$He^{2+} + e^- \rightarrow He^+ + 54.417\ eV \tag{12}$$

And, the overall reaction is

$$H[a_H] \rightarrow H\left[\frac{a_H}{3}\right] + 54.4\ eV + 54.4\ eV \tag{13}$$

Since the products of the catalysis reaction have binding energies of $m \cdot 27.2\ eV$, they may further serve as catalysts. Thus, further catalytic transitions may occur: $n = \frac{1}{3} \rightarrow \frac{1}{4}$, $\frac{1}{4} \rightarrow \frac{1}{5}$, and so on.

Electronic transitions to Rydberg states given by Eqs. (1) and (3) catalyzed by the resonant nonradiative transfer of $m \cdot 27.2\ eV$ would give rise to a series of emission lines of energies $q \cdot 13.6\ eV$ where q is an integer. It is further proposed that the photons that arise from hydrogen transitions may undergo inelastic helium scattering. That is, the catalytic reaction

$$H[a_H] \xrightarrow{He^+} H\left[\frac{a_H}{3}\right] + 54.4\ eV + 54.4\ eV \tag{14}$$

yields $54.4\ eV$ by Eq. (12) and a photon of $54.4\ eV$ (22.8 *nm*). Once emitted, the photon may be absorbed or scattered. When this photon strikes

$He(1s^2)$, $21.2\,eV$ may be absorbed in the excitation to $He(1s^1 2p^1)$. This leaves a $33.19\,eV$ ($37.4\,nm$) photon peak and a $21.2\,eV$ ($58.4\,nm$) photon from $He(1s^1 2p^1)$. Thus, for helium the inelastic scattered peak of $54.4\,eV$ photons from Eq. (11) is given by

$$E = 54.4\,eV - 21.21\,eV = 33.19\,eV\ (37.4\,nm) \tag{15}$$

A novel peak shown in Figures 7 and 8 was observed at $37.4\,nm$. Furthermore, the intensity of the $58.4\,nm$ peak corresponding to the spectra shown in Figure 8 was about 60,000 photons/sec. Thus, the transition $He(1s^2) \rightarrow He(1s^1 2p^1)$ dominated the inelastic scattering of EUV peaks. The general reaction is

$$photon\,(h\nu) + He(1s^2) \rightarrow He(1s^1 2p^1) + photon\,(h\nu - 21.21\,eV) \tag{16}$$

The two empirical series may be combined—one directly from Eqs. (1, 3) and the other indirectly with Eq. (16). The energies for the novel lines in order of energy are $13.6\,eV$, $27.2\,eV$, $40.8\,eV$, $54.4\,eV$, $81.6\,eV$, $95.2\,eV$, $108.8\,eV$, $122.4\,eV$ and $149.6\,eV$. The corresponding peaks are $91.2\,nm$, $45.6\,nm$, $30.4\,nm$, $37.4\,nm$, $20.5\,nm$, $13.03\,nm$, $14.15\,nm$, $10.13\,nm$, and $8.29\,nm$, respectively. Thus, the identified novel lines correspond to energies of $q \cdot 13.6\,eV$ where $q = 1,2,3,4,6,7,8,9,11$ or these lines inelastically scattered by helium atoms wherein $21.2\,eV$ was absorbed in the excitation of $He(1s^2)$ to $He(1s^1 2p^1)$. The values of q observed are consistent with those excepted based on Eq. (13) and the subsequent autocatalyzed reactions as discussed previously [2]. The satellite peak at $44.2\,nm$ show in Figure 7 and 2 may be due to multipole coupling as discussed elsewhere [8]. There is remarkable agreement between the data and the proposed transitions to fractional Rydberg states and these lines inelastically scattered by helium according to Eq. (16). All other peaks could be assigned to He I, He II, second order lines, or atomic or molecular hydrogen emission. No known lines of helium or hydrogen explain the $q \cdot 13.6\,eV$ related set of peaks.

B. Line broadening and T_e measurements

The Doppler-broadened line shape for atomic hydrogen has been studied on many sources such as hollow cathode [22-23] and rf [24-25] discharges. The method of Videnovic et al. [22] was used to calculate the energetic hydrogen atom densities and energies from the width of the

656.3 nm Balmer α line emitted from the hydrogen and helium-hydrogen mixture (90/10%) microwave plasmas shown in Figure 9. Gigosos et al. [26] have published a literature review of this method. The average helium-hydrogen Doppler half-width of $0.52 \pm 5\% \, nm$ was not appreciably changed with pressure. The corresponding energy of $180\text{-}210 \, eV$ and the number densities of $5 X 10^{14} \pm 20\% \, atoms/cm^3$, depending on the pressure, were significant compared to only $\approx 3 \, eV$ and $7 X 10^{13} \, atoms/cm^3$ for pure hydrogen, even though 10 times more hydrogen was present. Only $\approx 3 \, eV$ broadening was observed with xenon-hydrogen (90/10%) ruling out collisional broadening.

Similarly, the average electron temperature for helium-hydrogen plasma was $28{,}000 \pm 5\% \, K$. Whereas, the corresponding temperature of helium alone was only $6800 \pm 5\% \, K$, and hydrogen alone was $5500 \pm 5\% \, K$. No high electric field was present in our experiments.

We have assumed that Doppler broadening due to thermal motion was the dominant source to the extent that other sources may be neglected. This assumption was confirmed when each source was considered. In general, the experimental profile is a convolution of two Doppler profiles, an instrumental profile, the natural (lifetime) profile, Stark profiles, Van der Waals profiles, a resonance profile, and fine structure. The contribution from each source was determined to be below the limit of detection [10-11].

Furthermore, no hydrogen species, H^+, H_2^+, H_3^+, H^-, H, or H_2, responds to the microwave field; rather, only the electrons respond. But, the measured electron temperature was about 1 eV; whereas, the measured H temperature was $180\text{-}210 \, eV$. This requires that $T_H >>> T_e$. This result can not be explained by electron or external Stark broadening or electric field acceleration of charged species. The electron density was five orders of magnitude too low [10-11]. And, in microwave driven plasmas, there is no high electric field in a cathode fall region ($> 1 kV/cm$) to accelerate positive ions as proposed previously [22-25] to explain significant broadening in hydrogen containing plasmas driven at a high voltage electrodes. It is impossible for H or any H-containing ion which may give rise to H to have a higher temperature than the electrons in a microwave plasma. The observation of excessive Balmer line broadening in a microwave driven plasma requires a source of energy other than

that provided by the electric field.

C. Heat Loss Calorimeter Power measurements

A lower bound for the production of excess power by the rt-plasma is based on an analysis of the surface thermal conductance. Heat is lost from the plasma tube by natural convection, radiation, and conduction. The rate of heat loss is

$$Q = \int_A H(\mathbf{x}, \Delta T)\Delta T dA \tag{17}$$

where

$$\Delta T = T - T_\infty \tag{18}$$

is the local temperature rise of the tube surface above the ambient temperature, $\mathbf{x}$ denotes the position vector on the surface, and H is the local conductance for heat flow from the surface to the ambient. Because convection and radiation intensify with increasing surface temperature the conductance also increases:

$$\frac{\partial H}{\partial \Delta T} > 0 \tag{19}$$

Decomposing the conductance yields

$$H(\mathbf{x}, \Delta T) = \overline{H} + \delta H(\mathbf{x}, \Delta T) \tag{20}$$

where δH is the local deviation from the mean conductance

$$\overline{H} = \frac{1}{A}\int_A H(\mathbf{x}, \Delta T) dA \tag{21}$$

and A is the tube surface area. The rate of heat loss is then

$$Q = \overline{H}\int_A \Delta T dA + \int_A \delta H(\mathbf{x}, \Delta T)\Delta T dA \tag{22}$$

$$= \overline{H}[1 + \alpha]\int_A \Delta T dA \tag{23}$$

$$= \overline{H}[1 + \alpha]\overline{\Delta T}A \tag{24}$$

where the mean tube surface temperature rise is

$$\overline{\Delta T} = \frac{1}{A}\int_A \Delta T dA \tag{25}$$

and

$$\alpha = \frac{\int_A (\delta H/\overline{H})\Delta T dA}{\int_A \Delta T dA} \tag{26}$$

is a dimensionless measure of the deviation of the conductance from the mean value over the tube surface. If the variation of conductance is weak, α will be small compared with unity. The heat loss ratio for the power (no subscript) and control (subscript 0) plasmas is

$$\frac{Q}{Q_0} = \frac{\overline{H}}{\overline{H_0}} \frac{[1+\alpha]}{[1+\alpha_0]} \frac{\overline{\Delta T}}{\overline{\Delta T_0}} \tag{27}$$

Assuming similar distributions of conductance for both plasmas $\alpha \sim \alpha_0$ and

$$\frac{Q}{Q_0} = \frac{\overline{H}}{\overline{H_0}} \frac{\overline{\Delta T}}{\overline{\Delta T_0}} \tag{28}$$

Because H is an increasing function of the tube temperature and because the power plasma results in generally higher surface temperature

$$\overline{H} > \overline{H_0} \tag{29}$$

The ratio of heat loss rates is then

$$\frac{Q}{Q_0} > \frac{\overline{\Delta T}}{\overline{\Delta T_0}} \tag{30}$$

Surface temperature measurements for the helium-hydrogen and krypton control plasmas with 30 W input are shown in Figure 10 and summarized in Table 1. The mean temperature rise is

$$\overline{\Delta T} = \frac{1}{A}\int_A \Delta T dA = \frac{2}{A}\int_{A/2} \Delta T dA \tag{31}$$

$$\cong \frac{2}{A}\left(\Delta T_{z=0}\frac{\Delta A}{2} + \Delta T_{z=2}\Delta A + \Delta T_{z=4}\Delta A + \Delta T_{z=6}\Delta A + \Delta T_{z=8}\Delta A \right) \tag{32}$$

$$= \frac{2\Delta A}{A}\left(\frac{\Delta T_{z=0}}{2} + \Delta T_{z=2} + \Delta T_{z=4} + \Delta T_{z=6} + \Delta T_{z=8} \right) \tag{33}$$

where symmetry about the cavity position $z=0$ was used. With $\Delta A/A = 2/18 = 1/9$ the averages are

$$\overline{\Delta T_0} = 28.2°\text{C} \tag{34}$$

$$\overline{\Delta T} = 100.5°C \tag{35}$$

and the ratio of heat loss rates is

$$\frac{Q}{Q_0} > \frac{\overline{\Delta T}}{\overline{\Delta T_0}} = 3.6 \tag{36}$$

Given a constant input power of 30 W, Q_T for the helium-hydrogen plasma was 108 W and the Q_{ex} (Eq. (6)) was 78 W in 10 cm^3.

D. Calvet Calorimeter Power measurements

The Calvet voltage of the xenon plasma and two helium-hydrogen plasmas at steady state with 22 W of input power is shown in Figure 11. The Calvet voltage response to power ratio for xenon was 0.66 mV/W. The excess power from helium-hydrogen plasmas were very reproducible. The Calvet voltage response to power ratio was 1.8 mV/W. Using the xenon result in Eq. (10), the total plasma power was 60 W corresponding to 38 W of excess power (Eq. (6)). Since the plasma was about 1 cm in length, the plasma volume was 0.32 cm^3. The excess power density was very high, 120 W/cm^3.

Given a helium-hydrogen (95/5%) flow rate of 8.0 sccm and an excess power of 38 W, energy balances of over $-1.3 \times 10^5\ kJ/mole\ H_2$ ($660\ eV/H\ atom$) were measured. The reaction of hydrogen to form water which releases $-241.8\ kJ/mole\ H_2$ ($1.48\ eV/H\ atom$) is about 450 times less than that observed. The results indicate that once an atom given by Eqs (1) and (3) is formed by a catalyst, further catalytic transitions: $n = \frac{1}{3} \rightarrow \frac{1}{4}, \frac{1}{4} \rightarrow \frac{1}{5}$, and so on occur to a substantial extent. This is consistent with the previously given theory [15, 2], the reported series of lower-energy hydrogen lines with energies of $q \cdot 13.6\ eV$ where $q = 1,2,3,4,6,7,8,9,$ *or* 11 [2, 7-8], and previous studies which show very large energy balances [7, 9].

4. Conclusion

We report that novel emission lines were observed with energies of $q \cdot 13.6\ eV$ where $q = 1,2,3,4,6,7,8,9,11$ or these lines inelastically scattered by helium atoms wherein $21.2\ eV$ was absorbed in the excitation of $He\ (1s^2)$ to $He\ (1s^1 2p^1)$. These lines were identified as transitions to fractional Rydberg states of atomic hydrogen. An extremely high hydrogen-atom temperature of $180\text{-}210\ eV$ was observed with the presence of helium ion catalyst only with hydrogen present. Similarly, the average electron temperature for helium-hydrogen plasma was high, 28,000 K, compared to 6800 K for helium alone.

Using heat loss and Calvet calorimetry, excess power was observed

from the helium-hydrogen plasma compared to control xenon or krypton plasmas. For a 30 W input, the minimum thermal output power of the helium-hydrogen plasma was estimated by heat loss calorimetry to be 108 W corresponding to 78 W of excess power in 10 cm^3. With 22 W of input power, the total plasma power of the helium-hydrogen plasma measured by Calvet calorimetry was 60 W corresponding to 38 W of excess power in 0.32 cm^3. The excess power density and energy balance were very high, $120\ W/cm^3$ and $-1.3 \times 10^5\ kJ/mole\ H_2$, respectively. The results indicate that an new power source based on the catalysis of atomic hydrogen is not only possible, but is it competitive with internal combustion.

Acknowledgments

Special thanks to Y. Lu and T. Onuma for recording some spectra.

References

1. R. Mills, J. Dong, Y. Lu, "Observation of Extreme Ultraviolet Hydrogen Emission from Incandescently Heated Hydrogen Gas with Certain Catalysts", Int. J. Hydrogen Energy, Vol. 25, (2000), pp. 919-943.
2. R. Mills, P. Ray, "Spectral Emission of Fractional Quantum Energy Levels of Atomic Hydrogen from a Helium-Hydrogen Plasma and the Implications for Dark Matter", Int. J. Hydrogen Energy, Vol. 27, No. 3, pp. 301-322.
3. R. Mills, P. Ray, "Vibrational Spectral Emission of Fractional-Principal-Quantum-Energy-Level Hydrogen Molecular Ion", Int. J. Hydrogen Energy, Vol. 27, No. 5, (2002), pp. 533-564.
4. R. Mills, "Spectroscopic Identification of a Novel Catalytic Reaction of Atomic Hydrogen and the Hydride Ion Product", Int. J. Hydrogen Energy, Vol. 26, No. 10, (2001), pp. 1041-1058.
5. R. Mills, M. Nansteel, and Y. Lu, "Observation of Extreme Ultraviolet Hydrogen Emission from Incandescently Heated Hydrogen Gas with Strontium that Produced an Anomalous Optically Measured Power Balance", Int. J. Hydrogen Energy, Vol. 26, No. 4, (2001), pp. 309-326.
6. R. Mills, T. Onuma, and Y. Lu, "Formation of a Hydrogen Plasma from an

Incandescently Heated Hydrogen-Catalyst Gas Mixture with an Anomalous Afterglow Duration", Int. J. Hydrogen Energy, Vol. 26, No. 7, July, (2001), pp. 749-762.

7. R. L. Mills, P. Ray, B. Dhandapani, M. Nansteel, X. Chen, J. He, "New Power Source from Fractional Rydberg States of Atomic Hydrogen", Chem. Phys. Letts., in press.
8. R. L. Mills, P. Ray, B. Dhandapani, J. He, "Spectroscopic Identification of Fractional Rydberg States of Atomic Hydrogen", J. of Phys. Chem. (letter), submitted.
9. R. Mills, A. Voigt, P. Ray, M. Nanstell, "Measurement of Hydrogen Balmer Line Broadening and Thermal Power Balances of Noble Gas-Hydrogen Discharge Plasmas", Int. J. Hydrogen Energy, Vol. 27, No. 6. (2002), pp. 671-685.
10. R. L. Mills, P. Ray, B. Dhandapani, J. He, "Comparison of Excessive Balmer α Line Broadening of Glow Discharge and Microwave Hydrogen Plasmas with Certain Catalysts", Phys. Chem., submitted.
11. R. L. Mills, P. Ray, "Substantial Changes in the Characteristics of a Microwave Plasma Due to Combining Argon and Hydrogen", New Journal of Physics, in press.
12. R. Mills, N. Greenig, S. Hicks, "Optically Measured Power Balances of Anomalous Discharges of Mixtures of Argon, Hydrogen, and Potassium, Rubidium, Cesium, or Strontium Vapor", Int. J. Hydrogen Energy, Vol. 27, No. 6, (2002), pp. 651-670.
13. R. Mills, B. Dhandapani, M. Nansteel, J. He, T. Shannon, A. Echezuria, "Synthesis and Characterization of Novel Hydride Compounds", Int. J. of Hydrogen Energy, Vol. 26, No. 4, (2001), pp. 339-367.
14. R. Mayo, R. Mills, M. Nansteel, "Direct Plasmadynamic Conversion of Plasma Thermal Power to Electricity", IEEE Transactions on Plasma Science, submitted.
15. R. Mills, *The Grand Unified Theory of Classical Quantum Mechanics*, September 2001 Edition, BlackLight Power, Inc., Cranbury, New Jersey, Distributed by Amazon.com; posted at www.blacklightpower.com.
16. R. Mills, "The Grand Unified Theory of Classical Quantum Mechanics", Int. J. Hydrogen Energy, Vol. 27, No. 5, (2002), pp. 565-590.
17. R. Mills, The Nature of Free Electrons in Superfluid Helium--a Test of Quantum Mechanics and a Basis to Review its Foundations and Make a

Comparison to Classical Theory, Int. J. Hydrogen Energy, Vol. 26, No. 10, (2001), pp. 1059-1096.

18. N. V. Sidgwick, *The Chemical Elements and Their Compounds*, Volume I, Oxford, Clarendon Press, (1950), p.17.
19. M. D. Lamb, *Luminescence Spectroscopy*, Academic Press, London, (1978), p. 68.
20. H. R. Griem, *Principle of Plasma Spectroscopy*, Cambridge University Press, (1987).
21. M. C. Bradford, J. Phillips, J., Klanchar, Rev. Sci. Instrum., 66, (1), January, (1995), pp. 171-175.
22. I. R. Videnovic, N. Konjevic, M. M. Kuraica, "Spectroscopic investigations of a cathode fall region of the Grimm-type glow discharge", Spectrochimica Acta, Part B, Vol. 51, (1996), pp. 1707-1731.
23. S. Alexiou, E. Leboucher-Dalimier, "Hydrogen Balmer-α in dense plasmas", Phys, Rev. E, Vol. 60, No. 3, (1999), pp. 3436-3438.
24. S. Djurovic, J. R. Roberts, "Hydrogen Balmer alpha line shapes for hydrogen -argon mixtures in a low-pressure rf discharge", J. Appl. Phys., Vol. 74, No. 11, (1993), pp. 6558-6565.
25. S. B. Radovanov, K. Dzierzega, J. R. Roberts, J. K. Olthoff, Time-resolved Balmer-alpha emission from fast hydrogen atoms in low pressure, radio-frequency discharges in hydrogen", Appl. Phys. Lett., Vol. 66, No. 20, (1995), pp. 2637-2639.
26. M. A. Gigosos, V. Cardenoso, "New plasma diagnosis tables of hydrogen Stark broadening including ion dynamics", J. Phys. B: At. Mol. Opt. Phys., Vol. 29, (1996), pp. 4795-4838.

Table 1. Surface temperatures recorded on the helium-hydrogen and krypton control plasmas with 30 W input.

	ΔT [°C]	
z [cm]	Krypton	Helium-hydrogen
0	114.8	434.3
2	54.0	178.5
4	12.7	42.7
6	2.4	11.2
8	0.2	2.9

Figure Captions

Figure 1. The general system design of the heat loss calorimeter.

Figure 2. Schematic of the heat loss calorimeter showing the thermocouple placement on the external wall of the quartz tube plasma cell.

Figure 3. Schematic showing series-connected thermo-elements to illustrate the operating principle of a Calvet calorimeter.

Figure 4. The general system design of the Calvet calorimeter.

Figure 5. Cross section of the Calvet calorimeter with the Beenakker microwave cavity in insitu shown along the axis of the cavity. The components are : 1) oven, 2) Calvet cup, 3) thermopile, 4) aluminum shots, 5) Beenakker cavity, 6) microwave connector, 7) 5 mm O.D., 3 mm I.D. quartz plasma chamber, and 8) microwave cavity tuning stubs.

Figure 6. Cross section of Beenakker microwave cavity shown perpendicular to the axis of the cavity. The components are : 1) microwave input connector, 2) 5 mm O.D., 3 mm I.D. quartz plasma chamber, 3) Beenakker cavity, 4) 6.4 mm O.D. stainless steel flexible tube, 5) stainless steel elbow, and 6) microwave cavity tuning stubs.

Figure 7. The EUV spectra ($17.5-50\,nm$) of the microwave cell emission of the helium-hydrogen mixture (98/2%) (top curve) recorded at 20 Torr with a normal incidence EUV spectrometer and a CEM, and control helium (bottom curve) recorded at 20 Torr with a 4° grazing incidence EUV spectrometer and a CEM. Only known He I and He II peaks were observed with the helium control. Reproducible novel emission lines were observed at $45.6\,nm$ and $30.4\,nm$ with energies of $q \cdot 13.6\,eV$ where $q = 2\ or\ 3$ (Eqs. (1, 3)) and at $37.4\,nm$ and $20.5\,nm$ with energies of $q \cdot 13.6\,eV$ where $q = 4\ or\ 6$ that were inelastically scattered by helium atoms wherein $21.2\,eV$ was absorbed in the excitation of $He\,(1s^2)$ to $He\,(1s^1 2p^1)$ as proposed in Eq. (16).

Figure 8. The short wavelength EUV spectra ($5-65\,nm$) of the microwave cell emission of the helium-hydrogen mixture (98/2%) (top curve) and control hydrogen (bottom curve) recorded at 1 Torr with a normal incidence EUV spectrometer and a CEM. No hydrogen emission was observed in this region, and no instrument artifacts were observed. Reproducible novel emission lines were observed at $45.6\,nm$, $30.4\,nm$,

13.03 nm, 10.13 nm, and 8.29 nm with energies of $q \cdot 13.6\ eV$ where $q = 2, 3, 7, 9,$ *or* 11 and at 37.4 nm, 20.5 nm, and 14.15 nm with energies of $q \cdot 13.6\ eV$ where $q = 4, 6,$ *or* 8 that were inelastically scattered by helium atoms wherein 21.2 eV was absorbed in the excitation of $He\,(1s^2)$ to $He\,(1s^1 2p^1)$ as proposed in Eq. (16). The peak at 13.03 nm was observed as a weak shoulder on the 14.15 nm peak, and has been observed in repeated (non-presented) spectra.

Figure 9. The 656.3 nm Balmer α line width recorded with a high resolution ($\pm 0.006\ nm$) visible spectrometer on a helium-hydrogen (90/10%) and a hydrogen microwave discharge plasma. Significant broadening was observed corresponding to an average hydrogen atom temperature of 180 - 210 eV.

Figure 10. Surface temperature measurements for the helium-hydrogen and krypton control plasmas with 30 W input as a function of position along the tube. The minimum thermal output power of the helium-hydrogen plasma was estimated to be 108 W.

Figure 11. The Calvet voltage of the xenon and two helium-hydrogen plasmas at steady state with 22 W of input power. The Calvet voltage response to power ratio was for xenon was 0.66 mV/W; whereas, that of helium-hydrogen was 1.8 mV/W. The total plasma power of the helium-hydrogen plasma was 60 W corresponding to 38 W of excess power in 0.32 cm^3. The excess power density was very high, 120 W/cm^3.

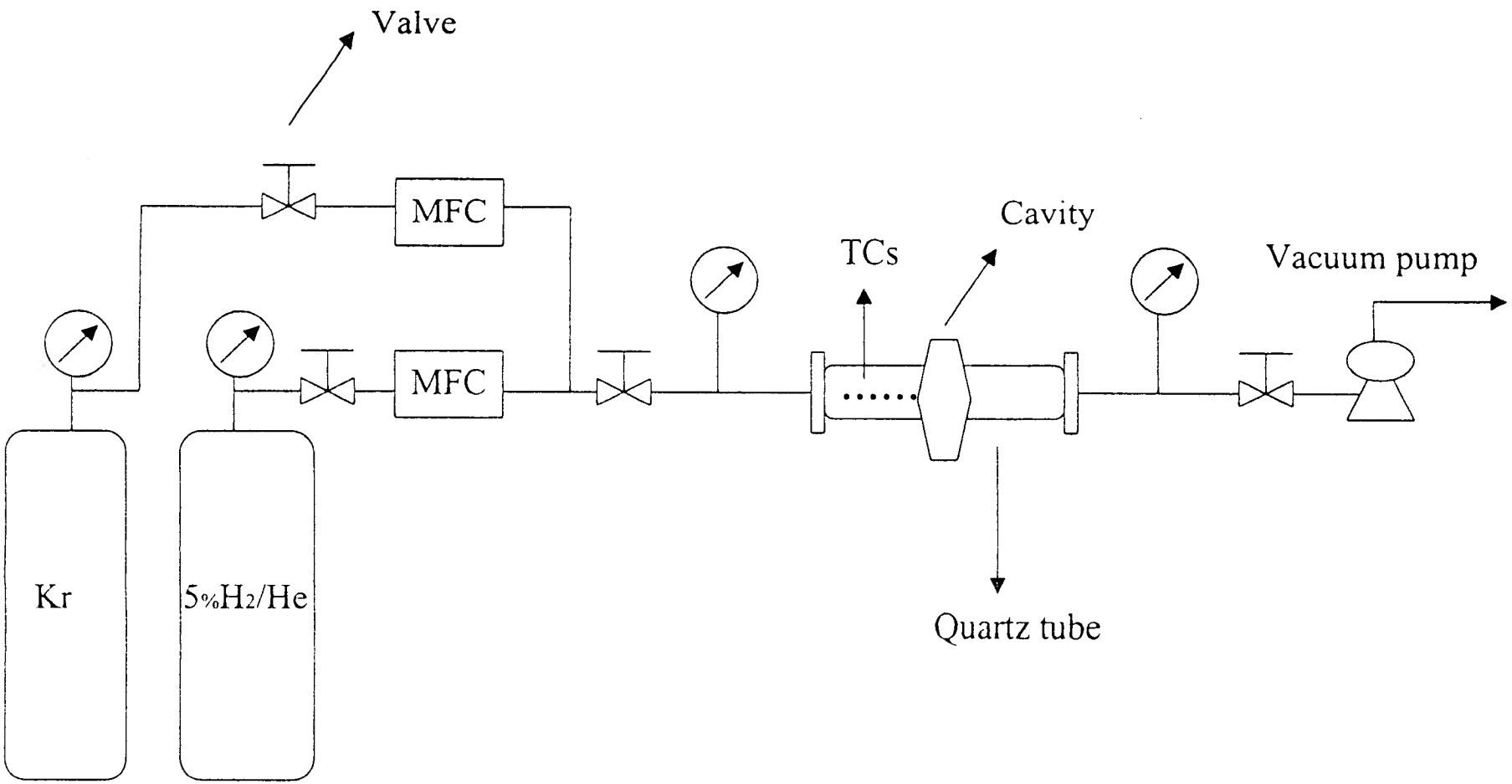

Fig. 1

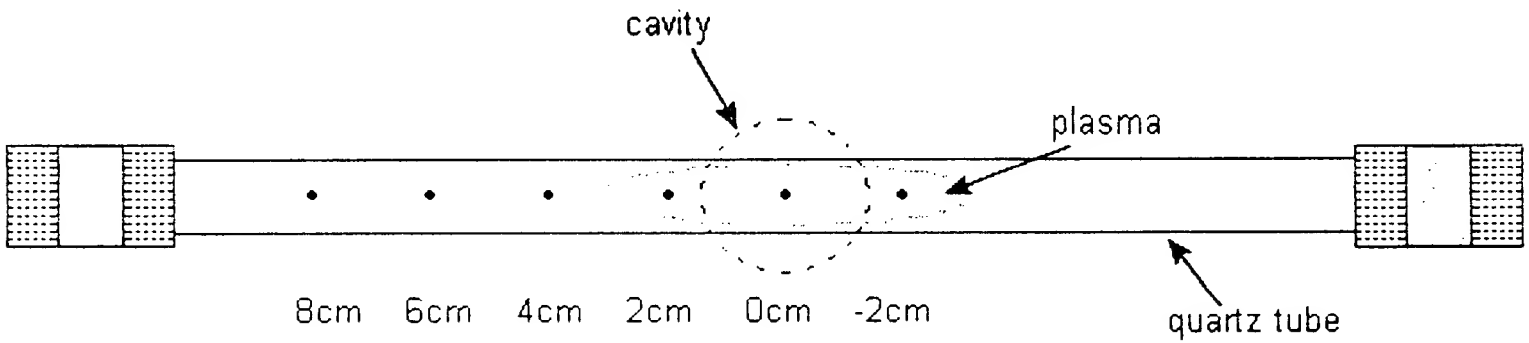

Fig. 2

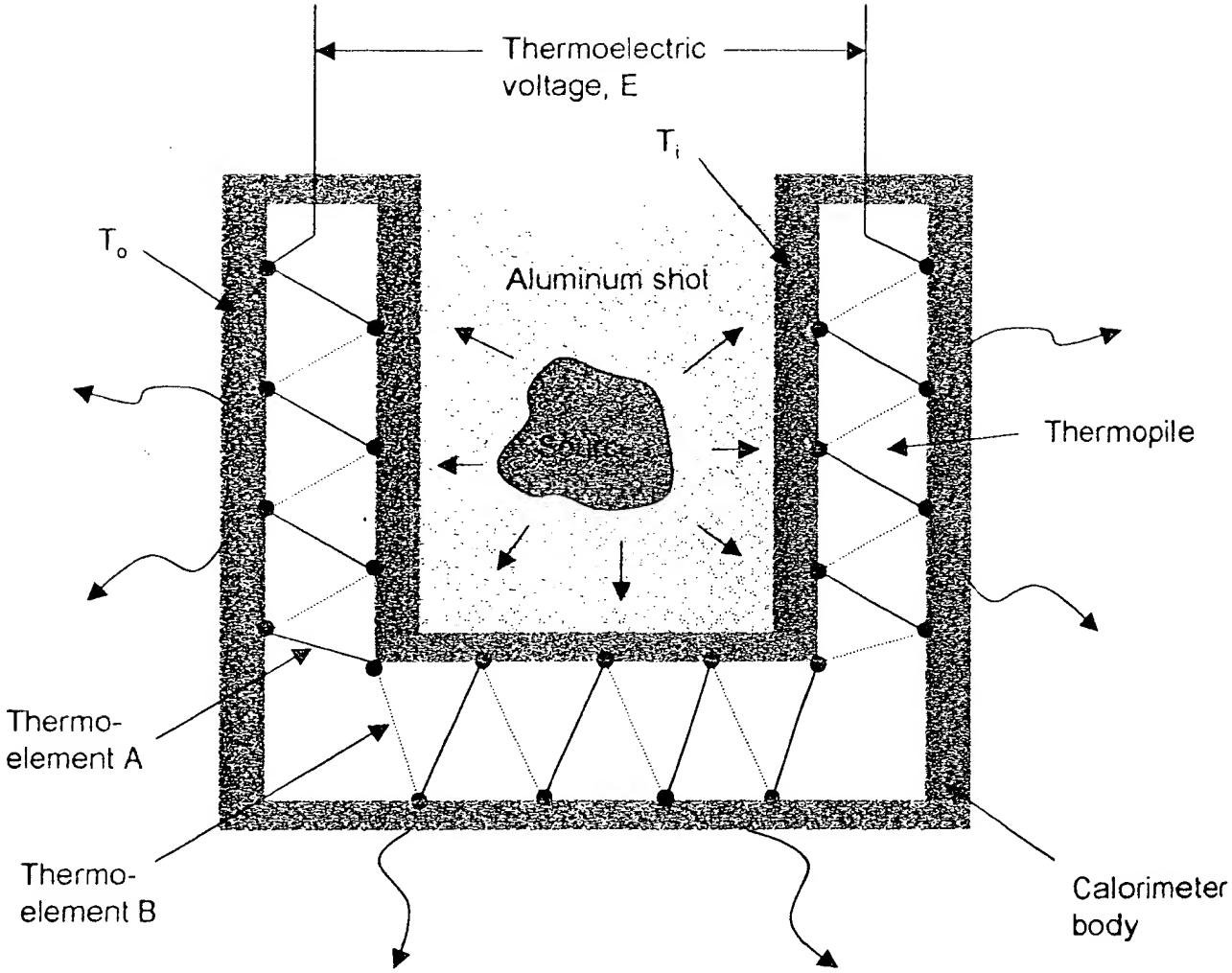
Thermoelectric
voltage, E
T_i
T_o
Aluminum shot
Source
Thermopile
Thermo-
element A
Thermo-
element B
Calorimeter
body

Fig. 3

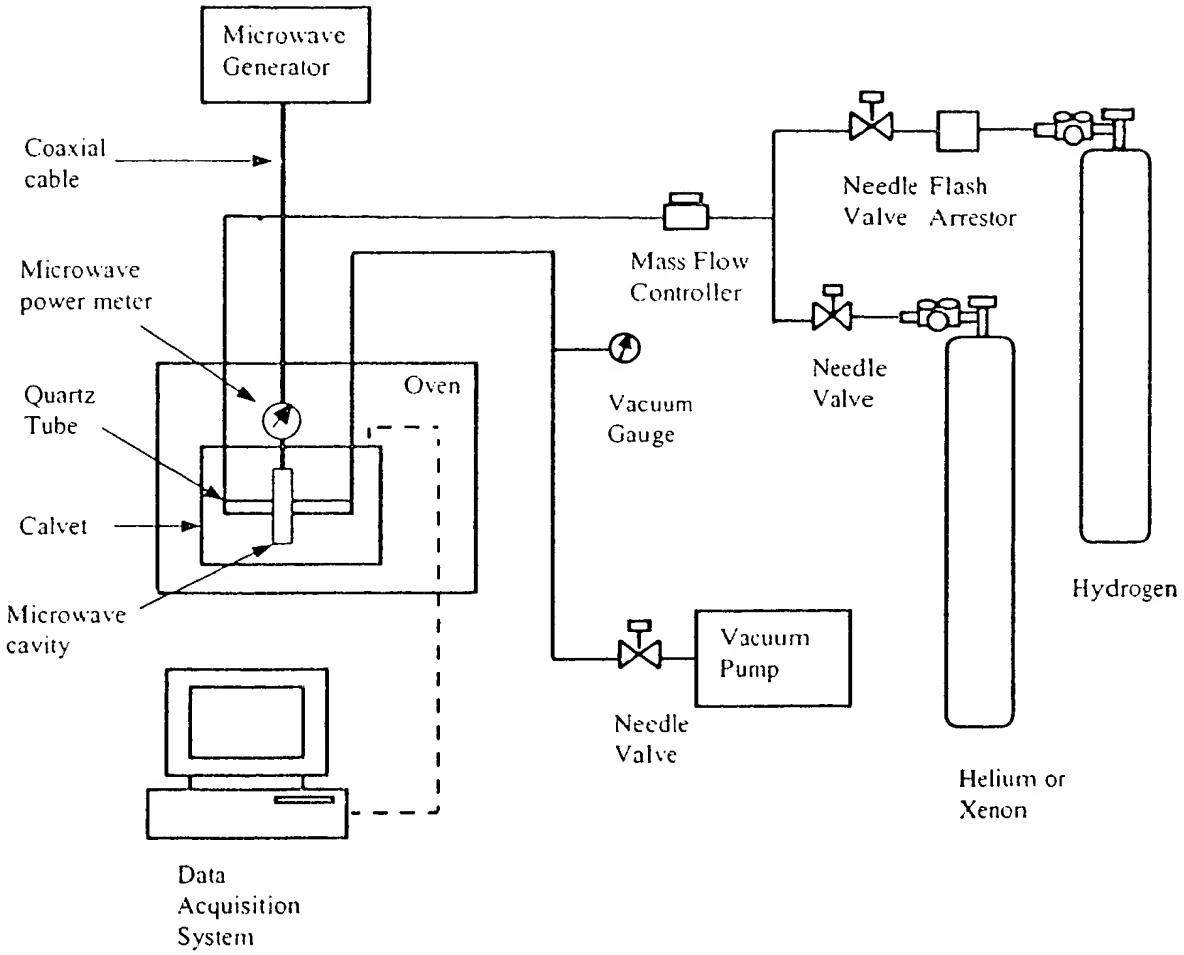
Microwave Generator
Coaxial cable
Microwave power meter
Quartz Tube
Calvet
Microwave cavity
Oven
Data Acquisition System
Mass Flow Controller
Vacuum Gauge
Vacuum Pump
Needle Valve
Needle Valve
Flash Arrestor
Hydrogen
Helium or Xenon

Fig. 4

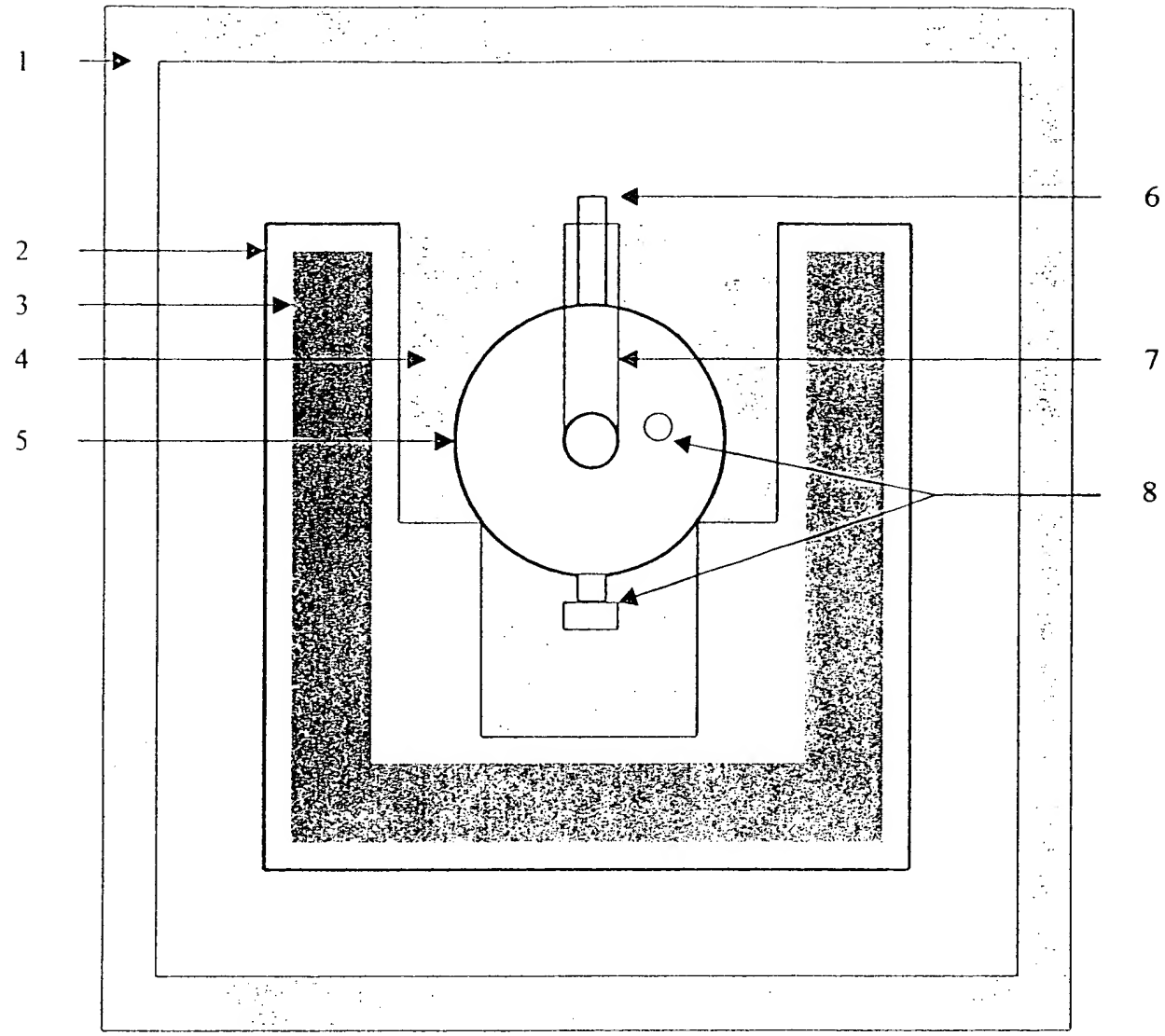

Schematic drawing of Calorimeter

Fig. 5

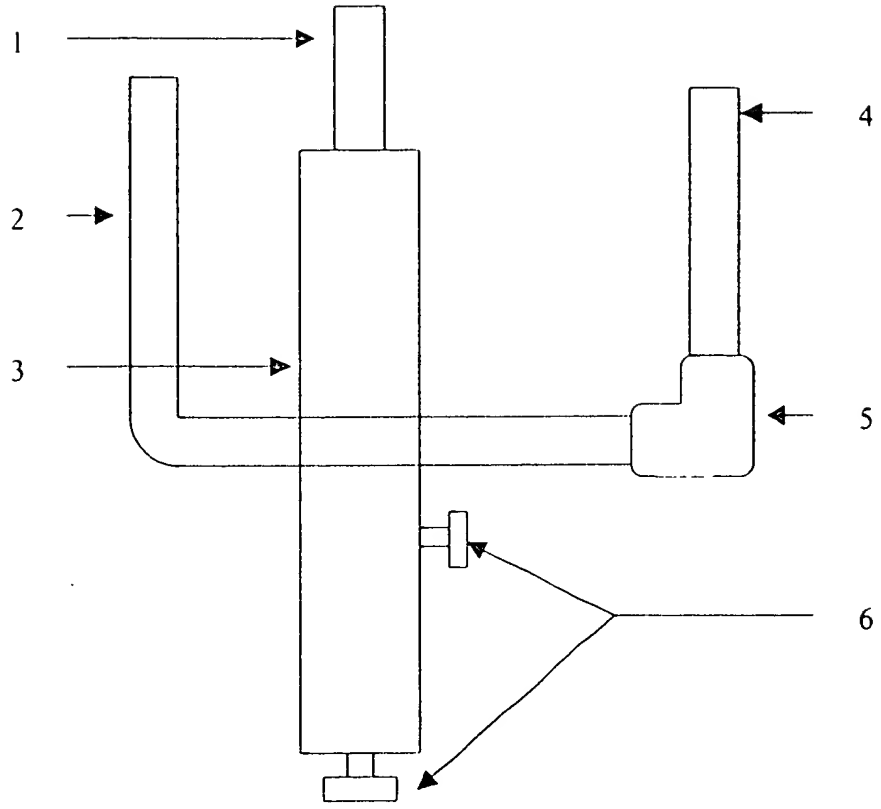

Side view of Beenakker cavity

Fig. 6

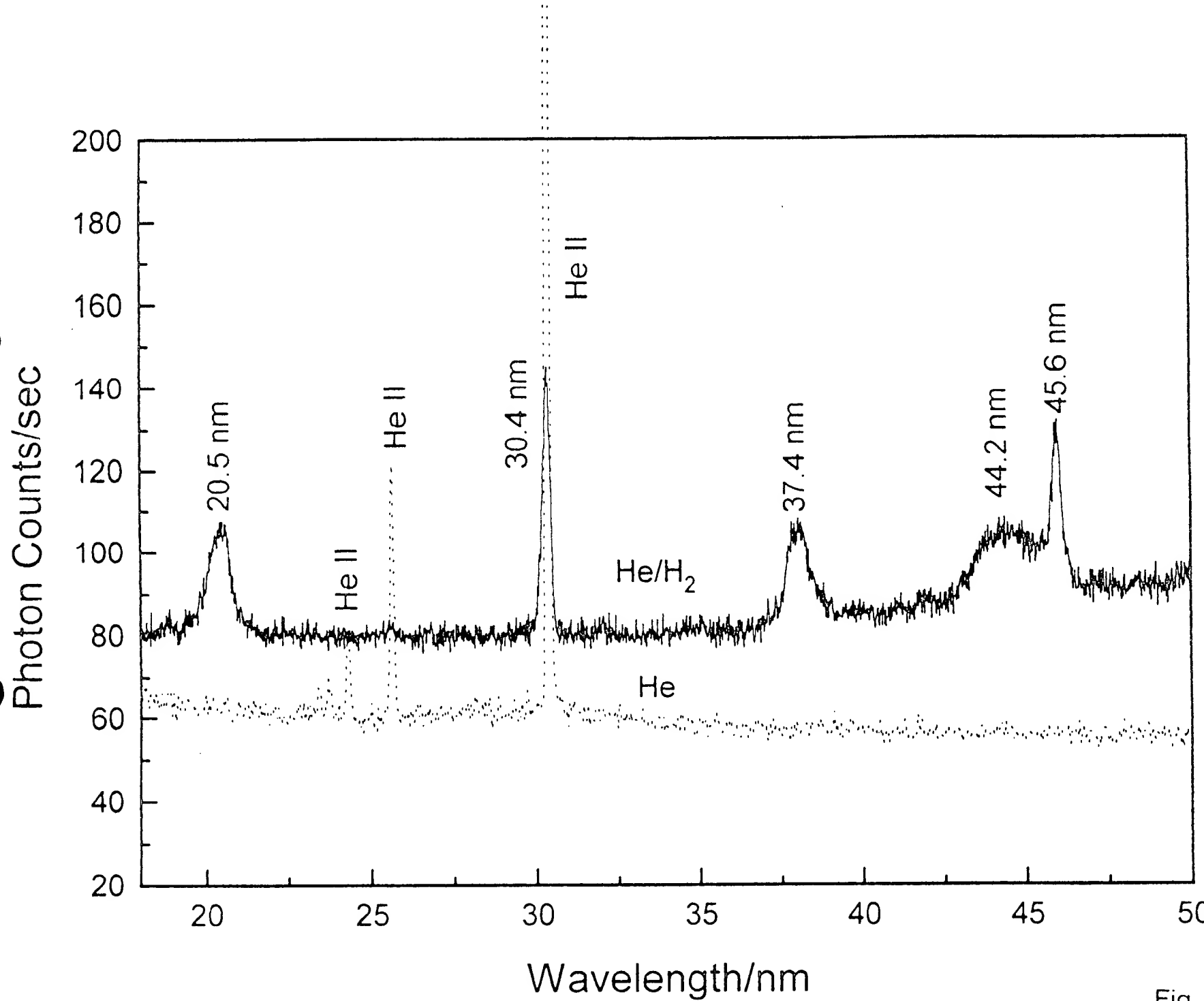
Photon Counts/sec
Wavelength/nm
200
180
160
140
120
100
80
60
40
20
20
25
30
35
40
45
50
20.5 nm
He II
He II
30.4 nm
He II
He/H2
37.4 nm
44.2 nm
45.6 nm
He

Fig. 7

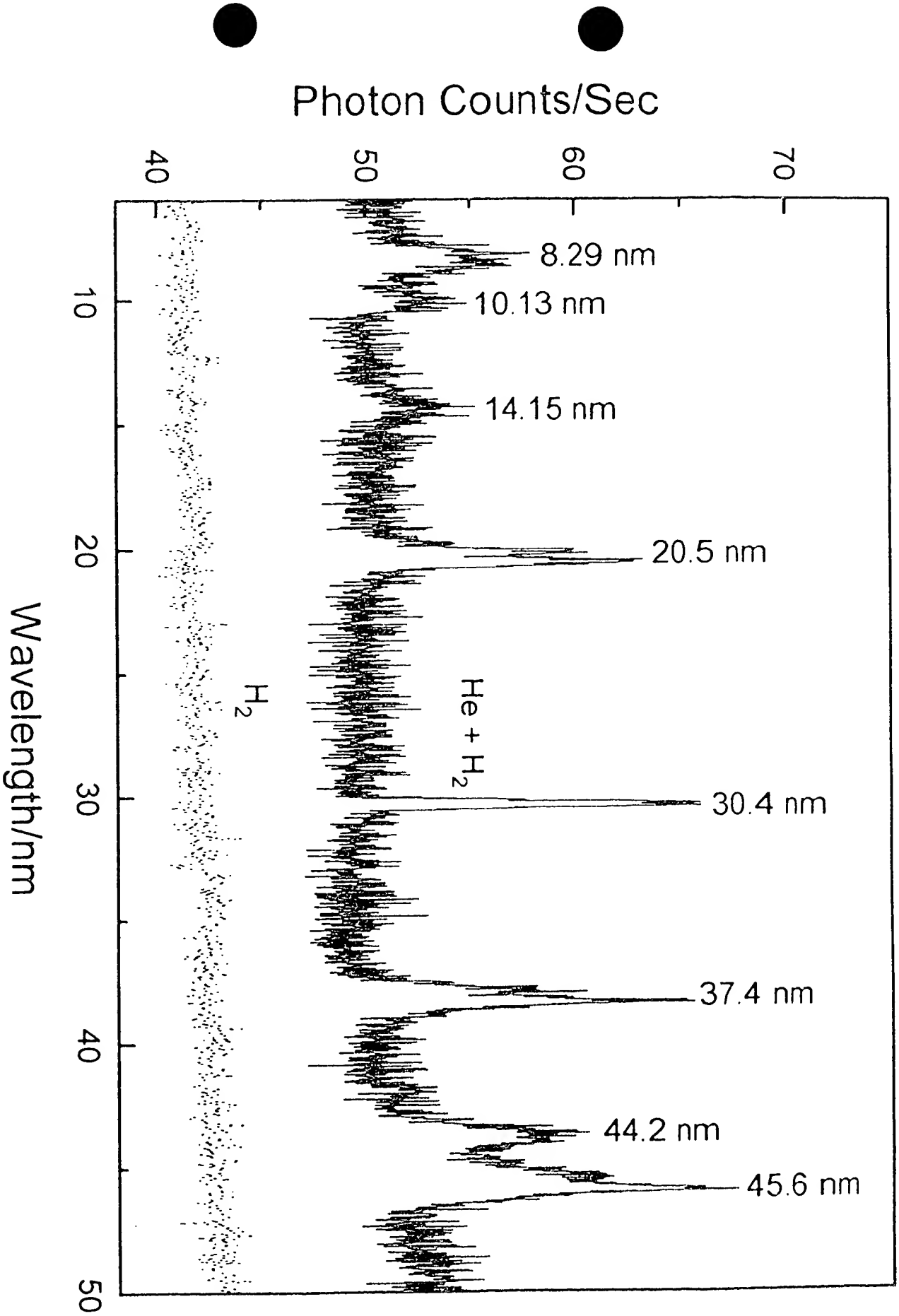
Photon Counts/Sec
40
50
60
70
Wavelength/nm
10
20
30
40
50
8.29 nm
10.13 nm
14.15 nm
20.5 nm
30.4 nm
37.4 nm
44.2 nm
45.6 nm
H2
He + H2

Fig. 8

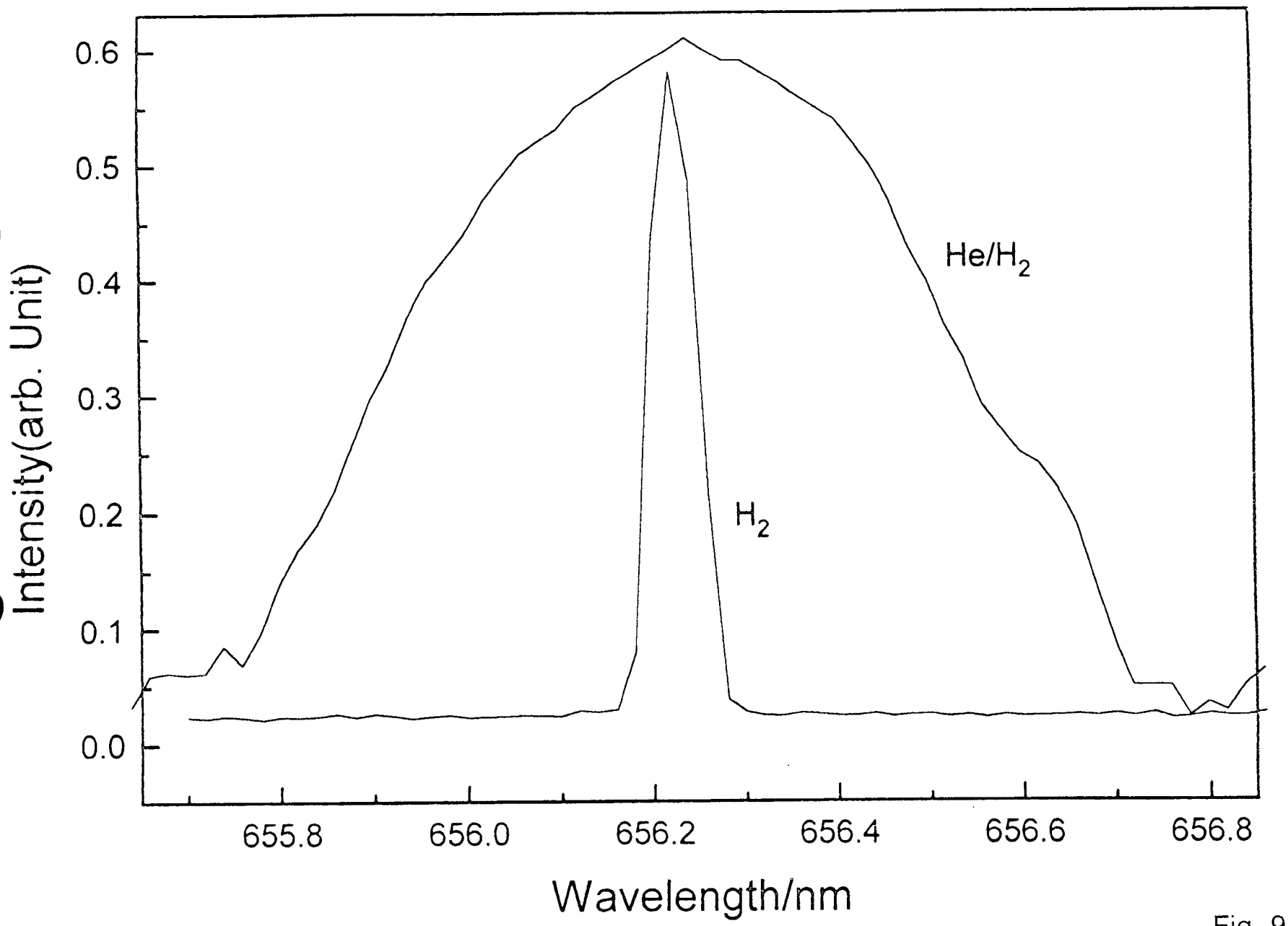
0.6
0.5
0.4
0.3
0.2
0.1
0.0
Intensity(arb. Unit)
He/H2
H2
655.8
656.0
656.2
656.4
656.6
656.8
Wavelength/nm

Fig. 9

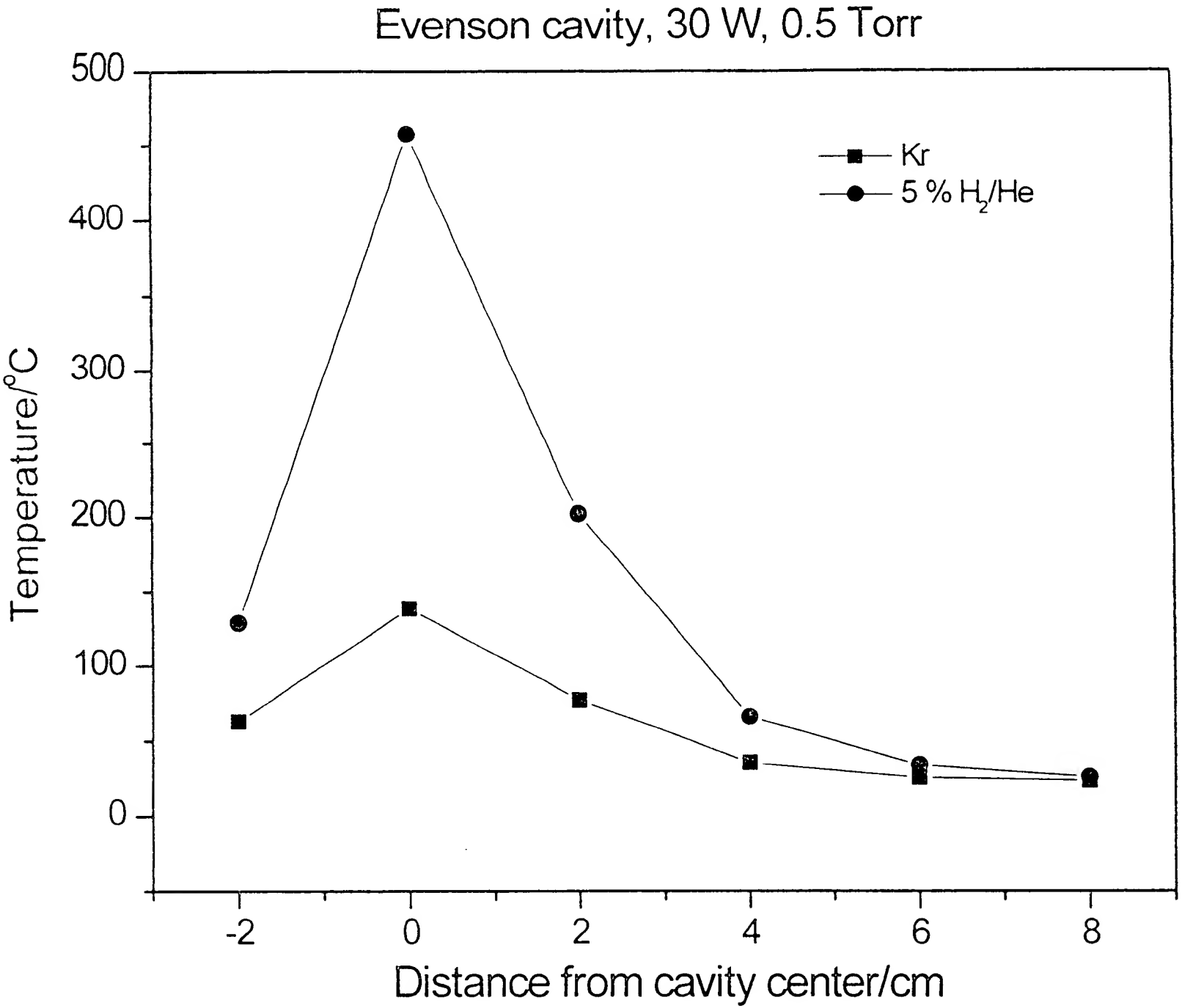
Evenson cavity, 30 W, 0.5 Torr
Kr
5 % H2/He
Temperature/°C
500
400
300
200
100
0
-2
0
2
4
6
8
Distance from cavity center/cm

Fig. 10

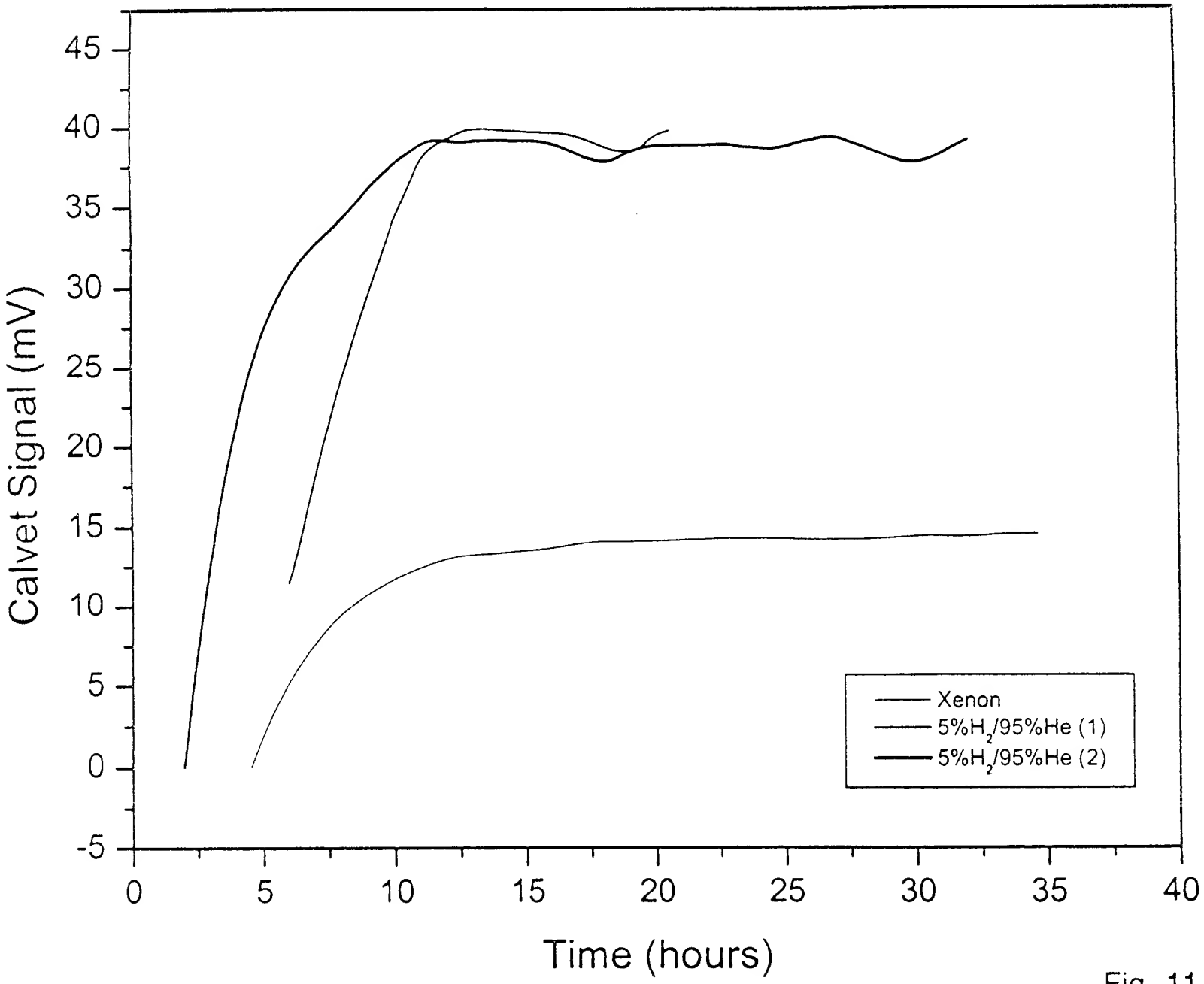
Calvet Signal (mV)
45
40
35
30
25
20
15
10
5
0
-5
0
5
10
15
20
25
30
35
40
Time (hours)
Xenon
5%H2/95%He (1)
5%H2/95%He (2)

Fig. 11